Using VBR Model in Fixed Speed Wind Turbines and Suggesting a New Method for Improving LVRT Capability

Hamid Rahimi Esfahani[1], Abbas Ketabi[2], Hamid Reza Mohammadi[3], Mohsen Rahimi Kelishadi[4]

[1] Instructor, Department of Power Engineering, Faculty of Electrical and Computer Engineering, University of Kashan, Kashan, Iran
h.rahimi@grad.kashanu.ac.ir
[2] Associate Professor, Department of Power Engineering, Faculty of Electrical and Computer Engineering, University of Kashan, Kashan, Iran
aketabi@kashanu.ac.ir
[3] Assistant Professor, Department of Power Engineering, Faculty of Electrical and Computer Engineering, University of Kashan, Kashan, Iran
mohammadi@kashanu.ac.ir
[4] Associate Professor, Department of Power Engineering, Faculty of Electrical and Computer Engineering, University of Kashan, Kashan, Iran
mrahimi@kashanu.ac.ir

Abstract:

Low Voltage Ride Through (LVRT) capability is essential for wind farms to avoid disconnection during low voltage and fault. In this study, both Voltage Behind Reactance (VBR) model and DQ model of Induction Generators (IGs) used in Fixed Speed Wind Turbines (FSWTs) are implemented and compared. Based on the appropriate model, a new method for enhancing Low Voltage Ride Through (LVRT) capability of FSWTs during balanced three-phase faults is proposed. This method is based on using a Synchronous Condenser (SC) with a Fuzzy Logic Controller (FLC). In order to have a good control of the system during the fault, the amount of injected reactive power produced by the SC is controlled through the FLC. Although using STATCOM is the most common method for LVRT capability enhancement in FSWTs, simulation results show that using the SC with the FLC in a three-phase fault leads to a better performance. Therefore, using the VBR model for the first time in FSWTs and suggesting the application of the SC with the FLC to improve LVRT capability are the novelties of this paper.

Keywords: Fixed Speed Wind Turbine; Fuzzy Logic Controller; Low Voltage Ride through Capability; Synchronous Condenser; VBR Model.

1. Introduction

As a result of growing penetration of wind farms, power grids have responded through developing particular grid codes to preserve their stability [1], [2]. One of the main grid codes is the LVRT capability. LVRT capability, in general, is the ability of Wind Turbine (WT) to stand against low voltage without reaching to unstable state which causes disconnection of WT from the grid [3]. Although FSWTs don't have the capability of reactive power adjustment and are confined to the LVRT requirements during grid faults, the advantages of these WTs such as simple structure, low cost, and high reliability make them popular for customers. In last activities during recent years, different LVRT methods have been proposed. There are many auxiliary devices to supply sufficient dynamic voltage support and improve the LVRT capability of FSWTs. The LVRT capability enhancement methods can be reviewed in two ways, which are:

1- Depending on the connection configuration;

2- depending on the rotor speed stability margins. Depending on the connection configuration, these methods can be classified into the series-connected solutions [4], [5], [6], [7], shunt-connected solutions [8], [9], [10], and hybrid-connected solutions [11], [12], [13], [14].

[1] Submission date: 06,03, 2019
Acceptance date: 01, 07, 2019
Corresponding author: Abbas Ketabi, Faculty of Electrical and Computer Engineering, University of Kashan, Kashan, Iran

During a fault or low voltage occurrence at stator terminals of a WTG, electromagnetic torque will minimize while mechanical torque still exists due to the non-stop wind blowing. This condition will produce a big torque difference in swing equation and causes the rotor speed to increase. If the fault or low voltage continues, it can cause the acceleration of the rotor of the WT and consequently the instability of the rotor speed.

Based on the aforementioned analysis, for improving rotor speed stability margin, using reactive power compensator devices is proposed. Several studies [15], [16], [17], [18] propose the usage of SVC equipment to supply the required reactive power of the generator during rotor acceleration. Also, as a reactive power compensator, STATCOM is used in [19], [20], [21] to supply IG with reactive power and the fuzzy controller is used in [22], [23], [24], [25]. According to [10] which deals with comparing SC and SVC performance, the results indicate that SVC injects greater reactive power and has a higher dynamic overall performance during minor faults such as single-phase to ground faults in weak grids. In contrast, for extreme faults such as three-phase to ground faults in stiff grids, the SC is more suitable and can bring the voltage to the nominal value faster and exhibit a higher dynamic overall performance. In [26] a comparison is made between SVC and STATCOM. The result of this comparison indicates that for enhancing the reactive power, STATCOM is more beneficial than SVC. Although using STATCOM is the most popular method among the mentioned solutions for LVRT capability improvement [19], [20], according to [27] SC has at least three advantages compared with STATCOM, which are:

Immediate time response to sudden voltage changes, contribution to system inertia, and contribution to system short-circuit power. Therefore, in this paper, a new method for LVRT capability enhancement in FSWTs using the SC is proposed. Besides the aforementioned advantages of the SC, simulation results show that for a three- phase to ground fault with a long duration using an SC with FLC has a better performance and is more compatible with new LVRT grid codes compared with STATCOM. The proposed FLC for the SC acts as soon as the fault occurs to compensate the need of reactive power.

When the DQ model of the IG used in the FSWT is interfaced with an external inductive network, to forestall the series connection of current sources with the inductive branches, the artificial numerical snubber circuits are often introduced at the IG terminals [28]. Another problem in DQ model is the transformations between DQ and ABC coordinates, which make the indirect interface between the IG model and the external network more complicated and the simulation may become inaccurate and less efficient [29].

In this paper, the VBR model is used for the IG in the FSWT. In this model, the IG stator is modeled as a three-phase controlled voltage sources behind constant and decoupled R-L branches. These branches are part of the external circuit which form a direct interface. The rotor subsystem is outside of the main electrical circuits, so the rotor model is presented in the DQ reference frame. Therefore, using two different ABC and DQ coordinates in stator and rotor equations improves the simulation efficiency [29]. In this paper, two case studies of an IG used in an FSWT interfaced with resistive and inductive networks are presented. Therefore, the advanced features of VBR modeling approach are demonstrated. Both simulation results are shown and compared in next section.

Due to the absence of the SC as a shunt compensating device in [30], applying the SC for improving LVRT capability of FSWTs and using the VBR model for the IG in the FSWT for the first time are the novelties of this paper.

This paper is organized into 6 sections. Section 2 describes the DQ model and VBR model for the IG in the FSWT and compares the simulation results for the two aforementioned models. This comparison leads to choosing the VBR model for the rest of the work. Section 3 deals with the modeling of the proposed system in MATLAB SIMULINK and any required descriptions. In section 4, the FLC strategies are presented. In section 5, the simulation results with and without using the SC during a balanced three-phase fault are presented and discussed. At the end of this section, a comparison between the SC and STATCOM for LVRT capability enhancement is made. Section 6 concludes the results.

2. Induction Generator Models

In [29] motor convention is used, in which positive machine currents are assumed to flow into the stator and rotor windings but in this paper, the generator convention is used according to WT application. Therefore, equations in [29] are used with minor changes and the same numerical data from [29] is used

for the IG in the WT application. For the sake of brevity, the equations are not repeated in this paper. Note that for both DQ and VBR models, a single rigid body system is described as the mechanical dynamics by the following equations [29]:

$$p\theta_r = \omega_r \quad (1)$$

$$p\omega_r = \frac{P}{2J}(T_e - T_m) \quad (2)$$

Where the operator $p = \frac{d}{dt}$; θ_r is the rotor position, ω_r is the rotor angular electrical speed, J is the moment of inertia, T_e, and T_m are electromagnetic torque and mechanical torque, respectively.

In this paper, due to the simulation of balanced three-phase faults and the absence of asymmetrical components of voltage and current, the zero sequence variables are not included. In power systems simulations, the DQ machine model is extensively used. However, due to the usage of DQ and ABC variables in the IG stator and the external network, respectively and their transformations, this model will be much less handy [29]. In the VBR model, due to expressing the machine, stator subsystem in ABC coordinates the direct interface with an external network is possible, while the DQ reference frame is used in the rotor subsystem [29].

2.1. Comparing DQ and VBR Models

In this section, these two models are simulated in an IG used in the FSWT and the better one is chosen for next simulations. As it was mentioned in the introduction section, the DQ model used for IG acts as a voltage-controlled current source, therefore the IG stator cannot be connected to the external inductive network directly and a snubber circuit is needed [29]. To have a good comparison, the induction machine modeled in [29] is selected and it is converted to an FSWT through using a 2-D Lookup Table to compute the turbine torque output (Tm) as a function of wind speed (w_Wind) and turbine speed (w_Turb) (see Fig. 1). According to [29], depending on the external resistive or inductive network, two case studies are conducted. A reference DQ model (for IG used in the FSWT) has been also implemented separately for the purpose of benchmark comparisons. The reference solution has been obtained using this model solved with 4th-order Runge-Kutta method using a very small fixed step of 1 μS, the same as [29].

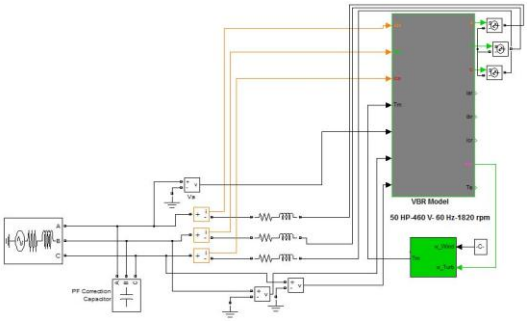

Fig (1): Implementation of the VBR Model of IG in an FSWT for SimPowerSystem in Matlab-Simulink

2.1.1. External Resistive Network

In this section, the IG in the FSWT is connected to a resistive network. The same time step of 10^{-4} S is used for both DQ and VBR models. The transient responses of these two models are overlapped in Figs. 2–4 and both are compared with the aforementioned reference solution. As seen in Figs. 2 – 4, the obtained simulation results in the VBR model match the reference solution very well while the DQ model doesn't match well and shows substantial errors.

In Figs. 2-4, the 'solid lines', 'dashed lines' and 'dotted lines' are used for 'reference model' 'DQ model' and 'VBR model', respectively.

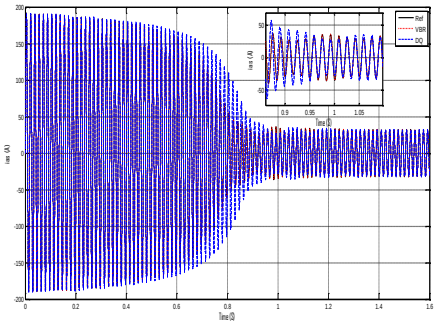

Fig (2): The Stator Current during the Startup Transient

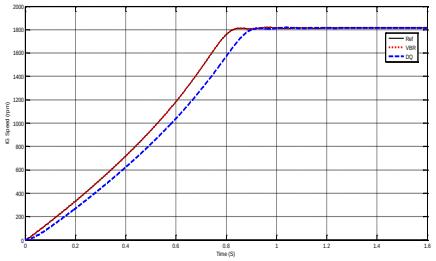

Fig (3): The IG Speed during the Startup Transient

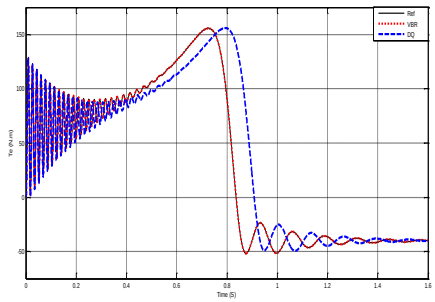

Fig (4): The IG Electromagnetic Torque during the Startup Transient

2.1.2. External Inductive Network

In the second case study, the IG shown in Fig. 1. is fed by an external inductive network. In interfacing with the external ABC phase coordinates, the DQ model acts as a voltage-controlled current source. Therefore, it is not possible to use the IG-network direct connection. To enable the direct connection, the artificial snubber which has high impedance is typically used [31]. In contrast, in the VBR model, no snubber circuit is required. Note that the omission of snubber circuits from the VBR model and the direct interface of the IG-network improves numerical accuracy and efficiency. These two model transient responses (using the same time step) are shown in Figs. 5-7. As seen in Figs. 5-7, both the DQ and VBR models converge to the reference solutions. However, the VBR model can use a much larger time-step (by two orders of magnitude). Therefore, the VBR model is more efficient in contrast to the DQ one [29]. Although DQ model has a better response in inductive mode compared with the resistive mode, the VBR response is better and more accurate in both cases. Therefore, VBR model is selected for the next section of this paper.

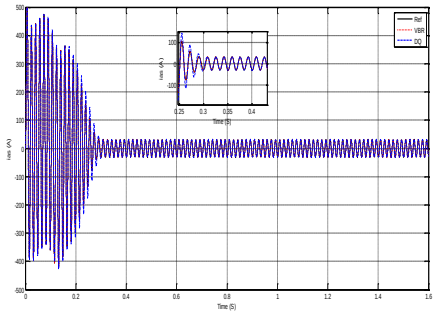

Fig (5): The Stator Current during the Startup Transient with the Inductive Network

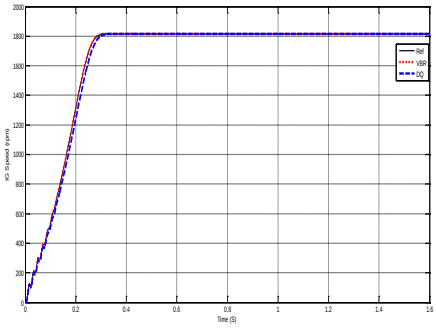

Fig (6): The IG Speed during the Startup Transient with the Inductive Network

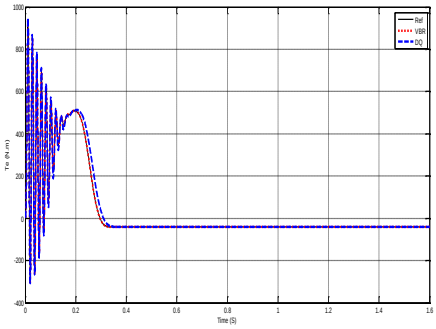

Fig (7): The IG Electromagnetic Torque during the Startup Transient with the Inductive Network

3. The Proposed System Description

In this section, the general schematic of an FSWT and an SC is shown in Fig. 8. in MATLAB SIMULINK. To have a better understanding of MATLAB-SIMULINK model in Fig. 8., it is described as:

An FSWT is fed at 480 V. The 480 V network is modeled by a simple R-L equivalent source and a 175 KW load. The IG is rated 275 KVA, 480 V and to compensate the need of reactive power in a severe three-phase to ground fault, the SC is rated 55 KVA, 480 V. The SC excitation is performed by the standard excitation block provided in the machine library.

The wind energy conversion system consists of Squirrel Cage Induction Generator (SCIG) with shunt connected capacitor bank to enhance the power factor [32]. The SC is not only replaced instead of power factor correction capacitors but also its excitation system controls the grid voltage at its nominal value.

As soon as occurring a fault, the SC produces more reactive power to compensate the fault harmful effects such as low voltage and need of more reactive power. A fuzzy controller is used which uses the WT speed and the 480 V bus voltage as inputs and produces an output to

control the switch connected to the field voltage of the SC. During the fault, the output of the fuzzy controller changes the field voltage (V_f) of the SC and causes dramatic changes in V_f which causes more production of reactive power and compensating fault harmful effects. The WTG in Fig. 8 includes a WT driving an IG which is directly connected to the 480 V bus and conforming a constant speed stall-controlled WTG (no pitch control) [33]. The WT block uses a 2-D Lookup Table to compute the turbine torque output (Tm) as a function of wind speed (w_Wind) and turbine speed (w_Turb). The detailed values of system parameters in Fig. 8 are presented in Appendix A [33]. The fault duration is equal to 9 cycles (150 mS). After this brief introduction of the system, now it is time to describe the control strategy in the next section.

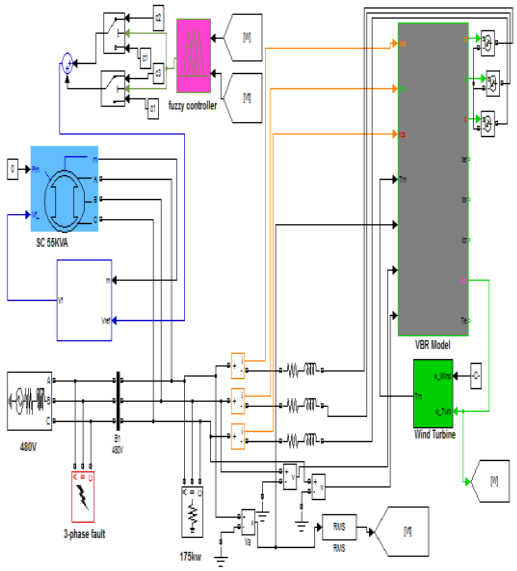

Fig (8): The Proposed System Model in MATLAB SIMULINK

4. Control Strategy

This section develops the control strategy of the SC for improving LVRT capability in FSWTs. So, the fuzzy controller design and its parameters, the rules and the membership functions are expressed. The proposed fuzzy controller is based on Mamdani's controller, which uses "if-then" rules for inference engine [34]. The rotor speed and the stator terminal voltage of the FSWT are considered as two inputs and also one output is produced. All inputs and the output are fuzzified by proper membership functions which are shown in Figs. 9-11.

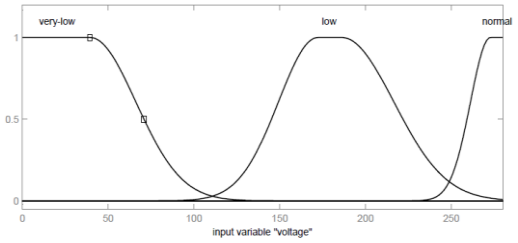

Fig (9): The Membership Function of the Input Variable 'Voltage'

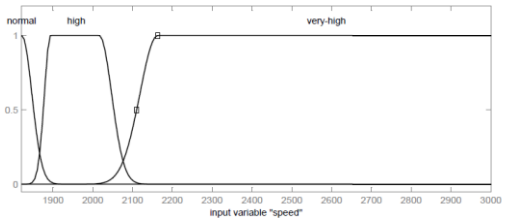

Fig (10): The Membership Function of the Input Variable 'Speed'

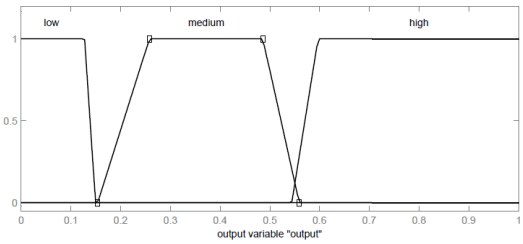

Fig (11): The Membership Function of the Output Variable

The rules containing inputs and output for this FLC are:

R1: If the speed is 'high' and the voltage is 'low' then the output is 'medium.'

R2: If the speed is 'very-high' and the voltage is 'very-low' then the output is 'high.'

R3: If the speed is 'normal' and the voltage is 'normal' then the output is 'low.

R4: If the speed is 'very-high' and the voltage is 'low' then the output is 'high.'

R5: If the speed is 'high' and the voltage is 'very-low' then the output is 'high.'

The logic is that when the rotor speed is high or very high and the stator voltage is low or very low, the system is in a critical condition, which needs the reactive power injection and depending on the fault severity and its depth, the amount of injected reactive power by the SC differs. As soon as a fault occurs, the output of FLC starts increasing and changes based on the fault depth passing the first or second threshold amount, which causes the inputs of the switches shown in Fig. 8. The changes in switches inputs increase the reference voltage value and consequently increase the field voltage of the SC for injecting more reactive power to the

system. After fault clearing, again the inputs of the switches are turned back to the previous values (below the threshold amounts), which change the amount of the field voltage of the SC to the normal value. The three-dimensional surface is shown In Fig. 12, which shows the relationship between inputs and the output of the FLC.

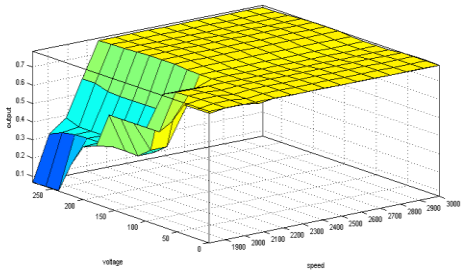

Fig (12): The FLC Inputs and Output Variables (Three-dimensional Graphics)

Based on Fig. 12, in Table 1, three different examples are presented for different states of the output. As seen in Table 1, when the output is 'medium', it is greater than the first threshold (0.25), and when the output is 'high', it is greater than the second threshold (0.65) and it is less than (0.25) for normal operation of the system. These examples are compatible with the fuzzy rules and show the correct FLC operation.

Table (1): Examples for different States of the Output of the FLC

Rotor speed value and state	Stator voltage value and state	Output value and state
1880 (high)	222 (low)	0.36 (medium)
2130 (very high)	59.6 (very low)	0.784 (high)
1850 (normal)	267 (normal)	0.09 (low)

After this explanation about the FLC operation, in next section, the simulation results are presented.

5. Simulation Results

In this paper, three different case studies are modeled and compared, while the three-phase fault is simulated. The duration of the fault is from 0.5 S to 0.65 S. The three case studies are described as:

1. three-phase fault without the SC connection at 480 V bus,

2. three-phase fault with the SC connection at 480 V bus,

3. three-phase fault with STATCOM connection at 480 V bus.

In the following, first, case studies '1', '2' are simulated and compared and finally, in the third case study, STATCOM is simulated and compared with the SC.

5.1. Comparing Case Studies '1', '2'

The simulation results of these two case studies are shown in Figs. 13-18.

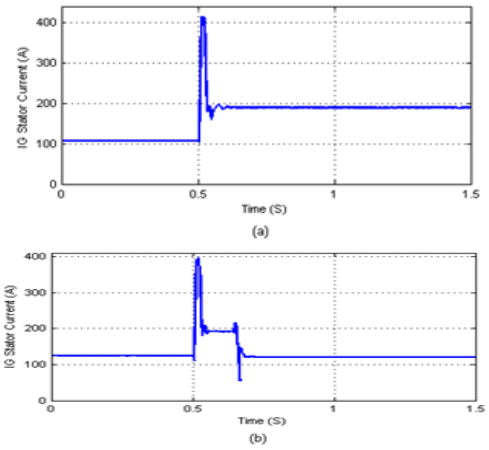

Fig. (13): The IG Stator Current (RMS) in the FSWT: (a) without the SC, (b) with the SC Connection at 480 V Bus

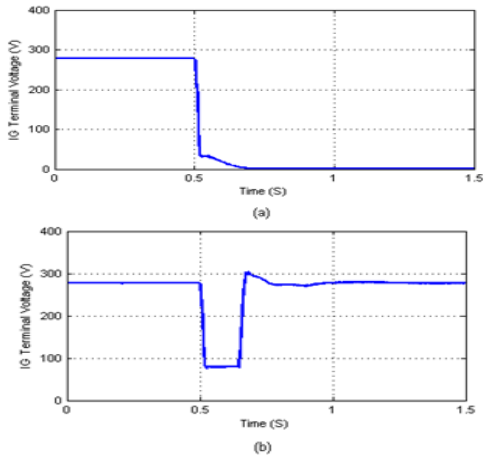

Fig (14): The IG Terminal Voltage (RMS) in the FSWT: (a) without the SC, (b) with the SC Connection at 480 V Bus

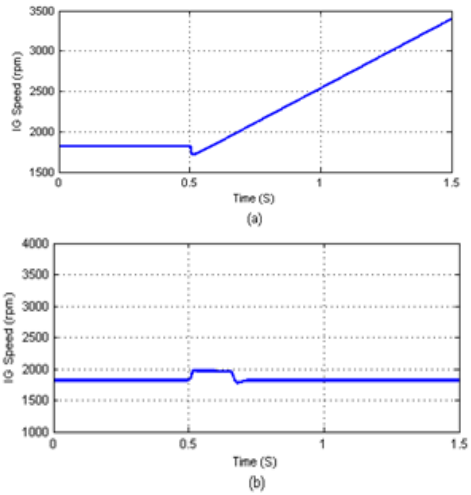

Fig (15): The IG Speed in the FSWT: (a) without the SC, (b) with the SC Connection at 480 V Bus

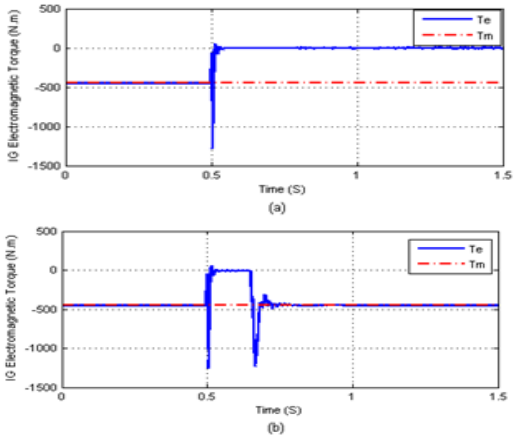

Fig (16): The IG Electromagnetic Torque in the FSWT: (a) without the SC, (b) with the SC Connection at 480 V Bus

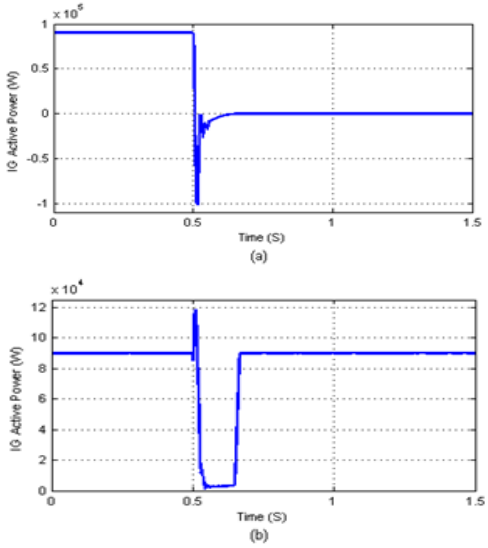

Fig (17): The IG Active Power (W) in the FSWT: (a) without the SC, (b) with the SC Connection at 480 V Bus

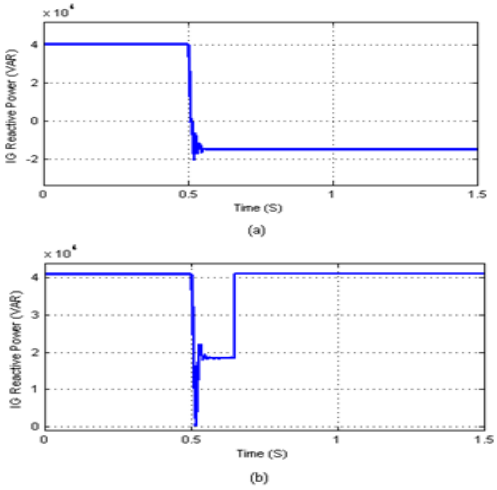

Fig (18): The IG Reactive Power (VAR) in the FSWT: (a) without the SC, (b) with the SC Connection at 480 V Bus

As shown in Figs. 13-18 (a) after fault clearance, all IG parameters in the FSWT reach to unstable state without turning back to their steady state. In contrast, in Figs. 13-18 (b) after fault clearance, all IG parameters in the FSWT are retrieved and turned back to their steady state. The reason for rotor speed instability in Fig. 15(a) is the extreme loss of electromagnetic torque in Fig. 16(a) (due to severe voltage dip in Fig. 14(a)) while mechanical torque is constant and as discussed in the introduction section, the high amount of difference between electrical torque and mechanical torque causes rotor of turbine to accelerate. The system instability causes the high value of stator current in Fig. 13(a) and active power to fall to zero in Fig. 17(a), while reactive power decreases in Fig. 18(a), which indicates the amount of required reactive power to improve the system stability.

From another point of view, by adding an SC to the system and supposing a three-phase fault the same as before, as shown in Figs. 13-15(b), after voltage retrieving, stator voltage, stator current and rotor speed in the FSWT, return to their steady state. In fact, in this case, the SC prevents electromagnetic torque loss to the unstable state by means of injecting required reactive power for IG (see Fig.16 (b)) and therefore preventing rotor unstable speed. In Figs. 17(b), 18(b), normal values of active and reactive power after fault clearing shows the successful operation of the SC during the fault. As seen in Fig. 19, during the fault, the field voltage of the SC increases dramatically and causes the injection of more reactive power to the system and after fault clearing, the field voltage of the SC decreases to the same amount

during normal operation of the system, which proves the correct operation of the FLC.

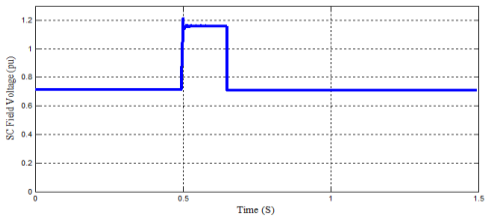

Fig (19): The SC Field Voltage (Vf (pu)).

5.2. Comparing the STATCOM and the SC Operation in a Three-phase Fault with Regard to The LVRT Curve

LVRT capability is the ability of an FSWT to survive low voltage without disconnecting from the grid that is all generating plants, which includes wind generator, and needs to have the capability of being connected during faults and low voltage conditions within certain restriction [35]. In order to prevent the disconnection of wind farms during network disturbances, the grid code requirements for LVRT are imposed by many countries. To define the requirements on the LVRT capability of grid-connected wind farms, China Electric Power Research Institute (CEPRI) developed revising Technical Rule for Connecting Wind Farms to Power System (GB/T 19963-2005) via inserting specific necessities on the LVRT curve. This rule has been applied since 30 June 2012 [36]. Fig. 20 shows the LVRT requirements for wind farms. According to this new standard, WTs should be able to preserve operating for 625 mS when the voltage of PCC falls to 20% of the nominal voltage. Also, in the new standard, WTs should stay connected to the power grid and keep on operating when the 90% of the nominal PCC voltage is retrieved in 2 seconds [36].

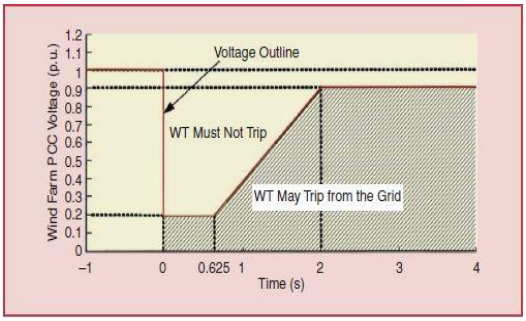

Fig (20): LVRT Requirements for Wind Farms [36].

In this subsection (third case study), first the same three-phase fault is applied on the FSWT and STATCOM and the SC operation are compared. Note that both STATCOM and the SC use FLC to improve LVRT capability and have the same 55 KVAR capacity of reactive power.

As shown in Fig. 21, the SC has a better performance in low voltage compensating, but both simulations for low voltage compensation are compatible with the LVRT curve (in Fig. 20).

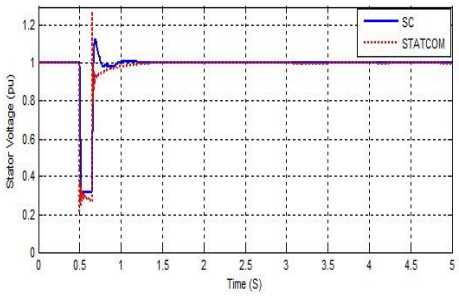

Fig (21): The SC and STATCOM Operational Effect on IG Terminal Voltage of Phase 'a' in the FSWT

In next step, the fault duration is longer (625 mS). As shown in Fig. 22, when the fault duration increases, according to the newest LVRT index (see Fig. 17), the FSWT with STATCOM should be disconnected from the grid, due to its low voltage (less than 20%) during this fault while the FSWT with SC can remain connected to the grid due to its higher voltage level (more than 20%).

In the final step, the reactive power capacity of STATCOM increases to 70 KVAR. This time STATCOM operation in Fig. 23, is compatible with LVRT index in Fig. 20, but the reactive power capacity of STATCOM increases dramatically. Therefore better performance of the SC in Three-phase faults (especially long duration three-phase faults) compared with STATCOM is clear as shown in Figs. 21-22.

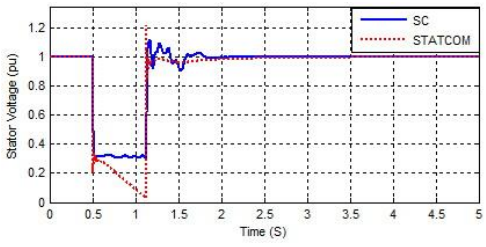

Fig (22): The SC and STATCOM Operational Effect on IG Terminal Voltage of Phase 'a' in the FSWT with Longer Fault Duration

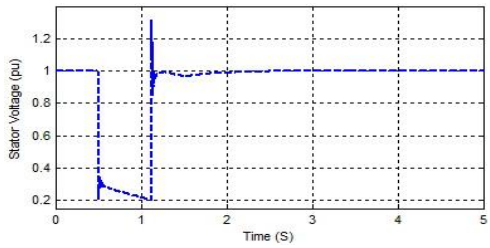

Fig (23): The 70 KVAR STATCOM Successful Operational Effect on IG Terminal Voltage of Phase 'a' in the FSWT with Longer Fault Duration

6. Conclusion

In this paper, first, the two DQ and VBR models for the IG used in an FSWT was simulated. The simulation results show that these two models are very similar in steady state, but due to simple equations for modeling, better response in the transient state, no need of snubber, and more accurate and efficient simulation, the VBR model is preferred and selected for next section. For decreasing harmful fault effects, using an SC with an FLC was suggested. By using a fuzzy controlled SC during fault occurrence, the production of reactive power increases dramatically to lessen harmful fault effects. After fault clearance time, the reactive power production by the SC decreases to the normal operational value. The increasing of the IG speed in an FSWT during a three-phase fault and the ability of the SC to control this high speed prove that this method is a good one for decreasing harmful fault effects which results in the proper operation of the system. Also, the simulation results show that in three-phase faults (especially with longer duration), the SC has a better operation compared with STATCOM, and is compatible with the new LVRT requirement for wind farms. This means that by using a fuzzy controlled SC, the FSWT can keep on working (even in a longer duration fault) without being disconnected from the grid. Despite downtrend of the FSWT applications, due to its simple structure and lower maintenance cost, the authors suggest using the VBR model for the first time in an FSWT and using a fuzzy controlled SC for LVRT capability enhancement.

Appendix A [33].

Table (2): IG Parameters

Main IG Parameters			
Pn(KVA)	275	H (S)	2
Vn(Vrms)	480	F (pu)	0
Rs(pu)	0.016	P	4
Lls(pu)	0.06	Rr'(pu)	0.015
Lm(pu)	3.5	Llr'(pu)	0.06

Table (3): SC Parameters

Main SG Parameters			
Pn(KVA)	55	Td'(s)	1.7
Xd(pu)	3.23	Td" (s)	0.008
Xd'(pu)	0.21	Tqo" (s)	0.004
Xd" (pu)	0.15	fn(Hz)	60
Xl(pu)	0.09	Rs(pu)	0.017
Xq(pu)	2.79	H(s)	1
Xq" (pu)	0.37	F (pu)	0
Exciter Parameters of SC			
Tr(s)	0.02	Ta(s)	0.001
Ka	300	Ke	1
Te(s)	0	Tb(s)	0
Tc(s)	0	Kf	0.001
Tf(s)	0.1	Efmin(pu)	-11.5
Efmax(pu)	11.5	Kp	0

References

[1] M. Cheng, S. Kato, and R. Shimada, "A novel method to improve low-voltage ride-through capability of wind turbine generators," *IEEJ Trans. Electr. Electron. Eng.*, Vol. 8, No. 5, pp. 522–528, Sep. 2013.

[2] H. Bastami, A. H. Abolmasoumi, and A. A. Ghadimi, "Stator voltage fault detection and optimal rotor current limiting in doubly fed induction generators," *Int. Trans. Electr. Energy Syst.*, Vol. 27, No. 5, pp. e2292-n/a, 2017.

[3] M. R. Shakarami, M. Joorabian, and E. Afzalan, "Enhancement Fault Ride-Through of DFIG with Applications of ISM Control for Balance and Unbalance Voltage Sag," *Comput. Intell. Electr. Eng.*, Vol. 10, No. 3, pp. 41–60, 2018.

[4] M. Farhadi-Kangarlu, E. Babaei, and F. Blaabjerg, "A comprehensive review of dynamic voltage restorers," *Int. J. Electr. Power Energy Syst.*, Vol. 92, pp. 136–155, 2017.

[5] D. Ramirez, S. Martinez, C. A. Platero, F. Blazquez, and R. M. De Castro, "Low-voltage ride-through capability for wind generators based on dynamic voltage restorers," *IEEE Trans. Energy Convers.*, Vol. 26, No. 1, pp. 195–203, 2011.

[6] M. Firouzi and G. B. Gharehpetian, "Improving fault ride-through capability of fixed-speed wind turbine by using bridge-type fault current limiter," *IEEE Trans. Energy Convers.*, Vol. 28, No. 2, pp. 361–369, 2013.

[7] G. Rashid and M. H. Ali, "A Modified Bridge-Type Fault Current Limiter for Fault Ride-Through Capacity Enhancement of

Fixed Speed Wind Generator," *IEEE Transactions on Energy Conversion*, Vol. 29, No. 2. pp. 527–534, 2014.

[8] M. M. A. Mahfouz and M. A. H. El-Sayed, "Static synchronous compensator sizing for enhancement of fault ride-through capability and voltage stabilisation of fixed speed wind farms," *IET Renewable Power Generation*, Vol. 8, No. 1. pp. 1–9, 2014.

[9] M. Noroozian, N. A. Petersson, B. Thorvaldson, A. B. Nilsson, and C. W. Taylor, "Benefits of SVC and STATCOM for electric utility application," *2003 IEEE PES Transmission and Distribution Conference and Exposition (IEEE Cat. No.03CH37495)*, Vol. 3. pp. 1143–1150 vol.3, 2003.

[10] S. Teleke, T. Abdulahovic, T. Thiringer, and J. Svensson, "Dynamic Performance Comparison of Synchronous Condenser and SVC," *IEEE Transactions on Power Delivery*, Vol. 23, No. 3. pp. 1606–1612, 2008.

[11] N. G. Jayanti, M. Basu, M. F. Conlon, and K. Gaughan, "Rating requirements of the unified power quality conditioner to integrate the fixedspeed induction generator-type wind generation to the grid," *IET Renewable Power Generation*, Vol. 3, No. 2. pp. 133–143, 2009.

[12] A. H. Moghadasi, A. Islam, and M. Amini, "LVRT capability assessment of FSIG-based wind turbine utilizing UPQC and SFCL," *2014 IEEE PES General Meeting | Conference & Exposition*. pp. 1–5, 2014.

[13] A. Moghadasi and A. Islam, "Enhancing LVRT capability of FSIG wind turbine using current source UPQC based on resistive SFCL," *2014 IEEE PES T&D Conference and Exposition*. pp. 1–5, 2014.

[14] P. H. Huang, M. S. El Moursi, W. Xiao, and J. L. Kirtley, "Fault Ride-Through Configuration and Transient Management Scheme for Self-Excited Induction Generator-Based Wind Turbine," *IEEE Transactions on Sustainable Energy*, Vol. 5, No. 1. pp. 148–159, 2014.

[15] N. Karpagam, D. Devaraj, and P. Subbaraj, "Improved fuzzy logic controller for SVC in power system damping using global signals," *Electr. Eng.*, Vol. 91, No. 7, pp. 395–404, 2010.

[16] R. Rahmani, M. F. Othman, A. A. Shojaei, and R. Yusof, "Static VAR compensator using recurrent neural network," *Electr. Eng.*, Vol. 96, No. 2, pp. 109–119, 2014.

[17] S.-Y. Lee and C.-J. Wu, "Reactive power compensation and load balancing for unbalanced three-phase four-wire system by a combined system of an SVC and a series active filter," *IEE Proceedings-Electric Power Appl.*, Vol. 147, No. 6, pp. 563–571, 2000.

[18] A. Gupta and P. R. Sharma, "Fuzzy based Svc auxiliary controller for damping low frequency oscillations in a power system," in *Confluence 2013: The Next Generation Information Technology Summit (4th International Conference)*, 2013, pp. 87–91.

[19] D. Ramirez, S. Martinez, F. Blazquez, and C. Carrero, "Use of STATCOM in wind farms with fixed-speed generators for grid code compliance," *Renew. Energy*, Vol. 37, No. 1, pp. 202–212, 2012.

[20] J. A. Suul, M. Molinas, and T. Undeland, "STATCOM-Based Indirect Torque Control of Induction Machines During Voltage Recovery After Grid Faults," *IEEE Transactions on Power Electronics*, Vol. 25, No. 5. pp. 1240–1250, 2010.

[21] Ismaili M. R., Bornapor M., Gholipour E., "Optimal placement of STATCOM for voltage control using partitioning methods and fuzzy adaptive modified particle swarm optimization algorithm," *Comput. Intell. Electr. Eng.*, Vol. 6, No. 4, pp. 49–62, 2016.

[22] H. M. Yassin, H. H. Hanafy, and M. M. Hallouda, "Enhancement low-voltage ride through capability of permanent magnet synchronous generator-based wind turbines using interval type-2 fuzzy control," *IET Renew. Power Gener.*, Vol. 10, No. 3, pp. 339–348, 2016.

[23] A. Sargolzaei, K. K. Yen, and M. N. Abdelghani, "Time-Delay Switch Attack on Load Frequency Control in Smart Grid," Vol. 5, pp. 55–64, 2013.

[24] H. Heydari-doostabad, R. Keypour, N. E. Member, and M. Khalghani, "New fuzzy control system design for maximum power point tracking of wind turbine," *18th Electric Power Distribution Conference*. pp. 1–6, 2013.

[25] Nikzad H. R., Izadfar R., "Design of an optimized Adaptive Neural Fuzzy controller for Constant Speed Wind Turbine," *Comput. Intell. Electr. Eng.*, vol. 7, no. 4, pp. 1–12, 2017.

[26] M. Molinas, J. A. Suul, and T. Undeland, "Low Voltage Ride Through of Wind Farms With Cage Generators: STATCOM Versus SVC," *IEEE Transactions on Power Electronics*, Vol. 23, No. 3. pp. 1104–1117, 2008.

[27] S. Kynev, G. Pilz, and H. Schmitt, "Comparison of modern STATCOM and

synchronous condenser for power transmission systems," *2016 IEEE Electr. Power Energy Conf. EPEC 2016*, 2016.

[28] R. Champagne, L. A. Dessaint, H. Fortin-Blanchette, and G. Sybille, "Analysis and validation of a real-time AC drive simulator," *IEEE Trans. Power Electron.*, Vol. 19, No. 2, pp. 336–345, 2004.

[29] L. Wang, J. Jatskevich, and S. C. Foroosh, "A VBR induction machine model implementation for SimPowerSystem toolbox in Matlab-Simulink," *IEEE Power Energy Soc. 2008 Gen. Meet. Convers. Deliv. Electr. Energy 21st Century, PES*, pp. 1–6, 2008.

[30] A. Moghadasi, A. Sarwat, and J. M. Guerrero, "A comprehensive review of low-voltage-ride-through methods for fixed-speed wind power generators," *Renew. Sustain. Energy Rev.*, Vol. 55, No. Supplement C, pp. 823–839, 2016.

[31] L. Wang, J. Jatskevich, and S. D. Pekarek, "Modeling of Induction Machines Using a Voltage-Behind-Reactance Formulation," *IEEE Transactions on Energy Conversion*, Vol. 23, No. 2. pp. 382–392, 2008.

[32] M. M. Aly, M. Abdel-Akher, S. M. Said, and T. Senjyu, "A developed control strategy for mitigating wind power generation transients using superconducting magnetic energy storage with reactive power support," *Int. J. Electr. Power Energy Syst.*, Vol. 83, No. Supplement C, pp. 485–494, 2016.

[33] R. Sebastián and R. P. Alzola, "Simulation of an isolated Wind Diesel System with battery energy storage," *Electr. Power Syst. Res.*, Vol. 81, No. 2, pp. 677–686, 2011.

[34] O. Cordón, "A historical review of evolutionary learning methods for Mamdani-type fuzzy rule-based systems: Designing interpretable genetic fuzzy systems," *Int. J. Approx. Reason.*, Vol. 52, No. 6, pp. 894–913, 2011.

[35] A. H. Kasem, E. F. El-Saadany, H. H. El-Tamaly, and M. A. A. Wahab, "A New Fault Ride-through Strategy for Doubly Fed Wind-Power Induction Generator," *2007 IEEE Canada Electrical Power Conference*. pp. 1–7, 2007.

[36] W. Weisheng *et al.*, "On the Road to Wind Power: China's Experience at Managing Disturbances with High Penetrations of Wind Generation," *IEEE Power Energy Mag.*, Vol. 14, No. 6, pp. 24–34, Nov. 2016.